IVYSPRING INTERNATIONAL PUBLISHER

Theranostics

2016; 6(10): 1557-1572. doi: 10.7150/thno.15231

Research Paper

Assessing Therapeutic Potential of Magnetic Mesoporous Nanoassemblies for Chemo-Resistant Tumors

Lina Pradhan[1, 4*], Bhushan Thakur[2*], Rohit Srivastava[3], Pritha Ray[2✉], Dhirendra Bahadur[4✉]

1. Centre for Research in Nanotechnology and Sciences, IIT Bombay, Mumbai, 400076,India.
2. Advance Centre for Treatment, Research and Education in Cancer, Tata Memorial Centre, Kharghar, Navi Mumbai, 410210, India.
3. Department of Biosciences and Bioengineering, IIT Bombay, Mumbai, 400076, India.
4. Department of Metallurgical Engineering and Materials Science, IIT Bombay, Mumbai, 400076 India.

*These authors contributed equally.

✉ Corresponding authors: Tel.: +91 22 2740 5119 (P. Ray). Tel.: +91 22 25767632 (D. Bahadur). E-mail addresses: pray@actrec.gov.in (P. Ray), dhirenb@iitb.ac.in (D. Bahadur).

Received: 2016.02.09; Accepted: 2016.04.28; Published: 2016.06.18

Abstract

Smart drug delivery system with strategic drug distribution is the future state-of-the-art treatment for any malignancy. To investigate therapeutic potential of such nanoparticle mediated delivery system, we examined the efficacy of dual drug-loaded, pH and thermo liable lipid coated mesoporous iron oxide-based magnetic nanoassemblies (DOX:TXL-LMMNA) in mice bearing both drug sensitive (A2780^S) and drug resistant (A2780-CisR) ovarian cancer tumor xenografts. In presence of an external AC magnetic field (ACMF), DOX:TXL-LMMNA particles disintegrate to release encapsulated drug due to hyperthermic temperatures (41-45 °C). *In vivo* bio distribution study utilizing the optical and magnetic properties of DOX:TXL-LMMNA particles demonstrated minimum organ specific toxicity. Noninvasive bioluminescence imaging of mice bearing A2780^S tumors and administered with DOX-TXL-LMMNA followed by the application of ACMF revealed 65% less luminescence signal and 80% mice showed complete tumor regression within eight days. A six months follow-up study revealed absence of relapse in 70% of the mice. Interestingly, the A2780-CisR tumors which did not respond to drug alone (DOX:TXL) showed 80% reduction in luminescence and tumor volume with DOX:TXL-LMMNA after thermo-chemotherapy within eight days. Cytotoxic effect of DOX:TXL-LMMNA particles was more pronounced in A2780-CisR cells than in their sensitive counterpart. Thus these novel stimuli sensitive nanoassemblies hold great promise for therapy resistant malignancies and future clinical applications.

Key words: Mesoporous magnetic nanoassembly, Dual drug carrier, Fluorescence and Bioluminescence imaging, Cisplatin resistance, Ovarian cancer xenografts, Combined thermo-chemotherapy effect.

1. Introduction

Cancer is one of the most fatal anomalies of human body whose cure is still a challenging task to the clinicians and scientists worldwide. Majority of the novel therapeutic strategies that were discovered and found to be effective against various malignancies in recent times fall short in treating radiation or chemo resistant diseases. Drug resistance is a multifactorial phenomenon comprising of abridged intracellular drug concentration, altered drug-target interaction, enhanced cell survival and defects in apoptotic pathways [1-3]. All these mechanisms may or may not be interdependent and hence pose a major road block to drug efficacy. This necessitates development of smarter treatment strategies, which will also be effective against therapy resistant malignancies. Nanoparticles based

multi-drug delivery systems promise to improve the efficacy, delivery and dose optimization over the existing chemotherapeutics in biomedical applications [1, 3-6]. Recent studies demonstrated that physico-chemical factors such as AC magnetic field, electric field, ultrasound, temperature and pH in combination with nano-carrier can act as triggers for chemotherapeutics release and exhibit synergistic effect on chemo-sensitive cancer [7-10]. Such strategy of combination therapy exhibits superior anti-tumor effects even against drug resistant tumor cells compared to photo/hyperthermia or chemo treatment alone [7]. However, efficacy of such stimuli sensitive nanoparticle mediated combination therapy on a chemoresistant cancer model is yet to be evaluated.

One of the major challenges in combined thermo-chemotherapy is to develop an efficient drug delivery system that amalgamates multiple drugs with controlled release, thereby increasing tumor regression capabilities [7, 11, 12]. It is challenging to integrate various requirements such as biocompatibility, good colloid stability, efficient multiple drug loading capacity and multi stimuli sensitivity for an ideal carrier molecule. An adjuvant externally applied AC magnetic field (ACMF) with superparamagnetic nanoassembly generates local hyperthermic temperature (41-45 °C) which enhances cellular permeability and retention effects (EPR). This improves the efficacy of drug accumulation at targeted lesions, decreases systemic toxicity, inducing apoptosis at the target tumor site synergistically [7, 8, 12-14]. Effect of such thermo-chemo therapy might become equally efficient against both sensitive and resistant tumors through targeting their biophysical characteristics.

Epithelial ovarian cancer is infamous for acquirement of resistance against the first line treatment regimen-cisplatin [15]. The current challenge lies in the management of platinum resistant ovarian tumor which is a leading cause of relapse and morbidity (5 year survival rate being 45%) [16]. Second line therapy involving paclitaxel, doxorubicin and etoposide drugs which produce significant toxicity and side effects, are the ultimate choice for these patients [17]. However, these drugs only increase overall survival without any significant increase in progression-free survival [17]. The lack of effective treatment modality against platinum resistant ovarian carcinoma thus till date remains an area of active research.

So far, there has been no study on the usage of magnetic nano-assemblies (which is an aggregation of single nanoparticles) for dual drug delivery as well as hyperthermia. These nano-assemblies have added advantages such as: higher magnetization, higher drug loading capacity for both hydrophilic and hydrophobic drugs and good colloidal stability in different solution over single nanoparticles.

Here, we report a smart pH- and thermo liable drug-delivery system that consists of a thin lipid layer with mesoporous magnetite nanoassemblies (LMMNA) as an effective therapeutic regimen against platinum resistant ovarian carcinoma. These nanoassemblies are capable of carrying and simultaneously delivering two anticancer drugs after suitable temperature or pH stimulation. As reported by us earlier, these LMMNA are characterized with high loading efficiency of hydrophilic doxorubicin hydrochloride (DOX) and hydrophobic paclitaxel (TXL) [18]. In the present study, cytotoxic effects of these particles were first tested in combination with hyperthermia against sensitive ($A2780^S$) and cisplatin-resistant (A2780-CisR) ovarian cancer cells. Interestingly, the particles produced higher lethality as compared to drug alone in A2780-CisR cells but not in $A2780^S$ cells. Next these LMMNA have been explored as a dual drug delivery system (DOX:TXL-LMMNA) for *in vivo* bio distribution and thermo-chemotherapeutic effects in tumor bearing mice through fluorescence and bioluminescence imaging (Scheme 1). Bio distribution and long term effect of these non-targeted nanoparticles were studied in mice by optical fluorescence imaging, transmission electron microscopy (TEM) of tissues and by measuring the "Fe" concentrations of vital organs through ICP-AES and magnetic measurement. Real time monitoring of the combined thermo-chemotherapy with DOX:TXL-LMMNA particles by optical imaging showed significant decrease in bioluminescence signal and tumour volume in comparison to control group for both $A2780^S$ and A2780-CisR tumor models. The efficacy was more pronounced in platinum resistant tumors as compared to drug alone treatment and in the sensitive tumors. Notably we did not observe any tumor relapse in 70% of the mice even after six months of completion of therapy. This is probably the first report and validation of a smart and stimuli sensitive magneto-nanoassembly system that shows enhanced toxicity against cisplatin resistant ovarian tumor xenografts using noninvasive optical imaging.

2. Experimental procedure

Preparation and characterization of DOX:TXL-LMMNA

MMNA and LMMNA preparation and characterization were described by us previously [18]. To load doxorubicin (Sigma Aldrich) into MMNA

particles, aquous solution of doxorubicin (500 µg/ml) was added to a suspension of 10 mg/ml of MMNA. Post overnight incubation, the DOX-MMNA were collected by centrifugation at 6720g for 10 min and stored at 4 °C for further experiments [18]. The concentration of unloaded drug in the supernatant was measured from the fluorescence spectra as described earlier. The percentage entrapment efficiency was calculated using the following calculation.

$$\%\ \text{entrapment efficiency} = \frac{Ic-Sc}{Ic} \times 100; \qquad \ldots(1)$$

where *Ic* and *Sc* are the respective initial concentrations of the DOX added and the DOX content of the supernatant.

Further dual drug–loaded (DOX and TXL) LMMNA (DOX:TXL-LMMNA) were prepared by the thin film hydration method described earlier [18]. Briefly, 2 mg of preloaded DOX-MMNA (containing equivalent of 80 µg DOX) was added into the lipid mixture of DPPC, Chol. and DSPE-PEG_{2000} in a 5:2:2 w/w ratio. For dual drug-encapsulated LMMNA, TXL (100 µg) was added concurrently to the synthesis of DOX-LMMNA. The encapsulation efficiency of DOX and TXL in LMMNA (labelled as DOX:TXL-LMMNA) was determined using UV-visible spectrophotometer (Super Aurius CE3021, Cecil Instruments, UK). The encapsulation efficiency and loading capacity of the drugs were calculated on the 5:2:2:2 w/w ratio of DOX:TXL-LMMNA with the initially added amount of the drug during the loading process using the following relations: (Eqn. 1) and,

$$\text{loading capacity} = \frac{\text{amount of drug incorporated in LMMNA (mg)}}{\text{LMMNA mass (mg)}}; \qquad \ldots(2)$$

Cell culture

A2780^S (human ovarian cancer cells) cell line was obtained from ATCC, USA. Cisplatin resistant counterpart for A2780 (A2780-CisR) was described earlier (Gaikwad et al. [19]). The cells were grown in Dulbecco's Modified Eagle's Medium (DMEM; HiMedia) supplemented with 10% fetal bovine serum (HiMedia) and 1% antibiotic antimycotic solution (HiMedia) in a humidified incubator at 37 °C, 5% CO_2. The resistant cells were maintained in 500 ng/ml of cisplatin.

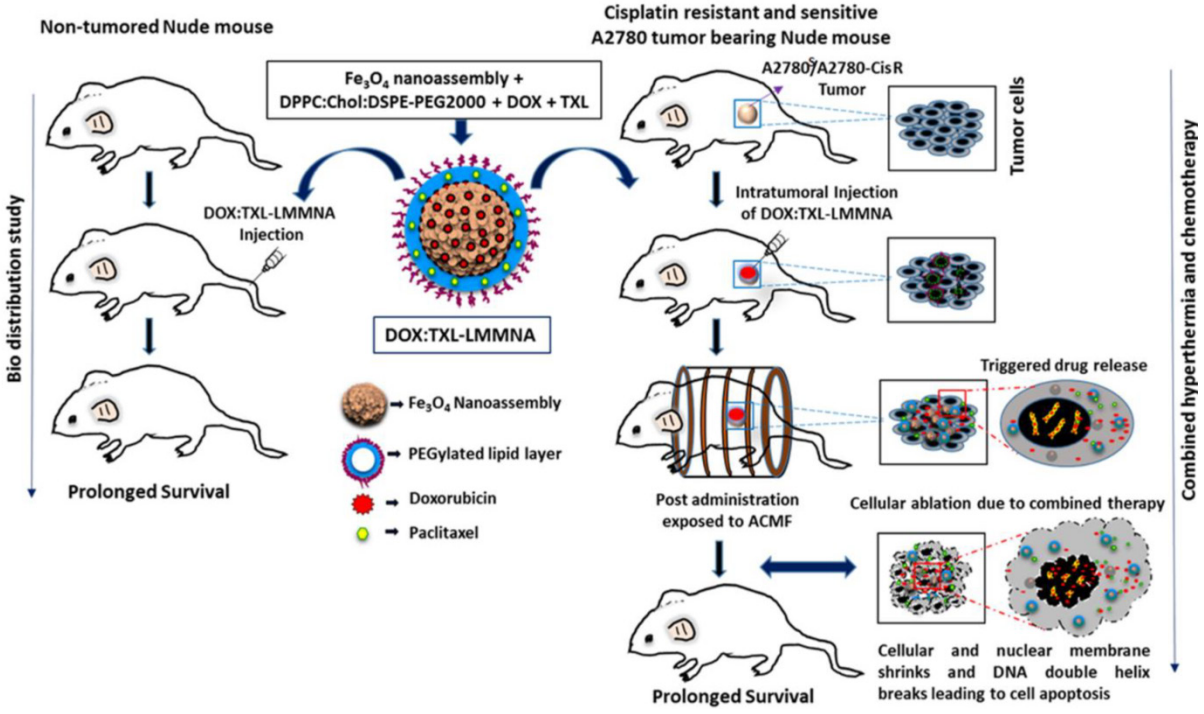

Scheme 1. Illustration of *in vivo* bio distribution in non-tumored mice and combined hyperthermia and chemotherapy with DOX:TXL-LMMNA as a dual drug delivery system on sensitive A2780^S and A2780-CisR tumor xenografts mice. The combination treatment of intratumoral injection of DOX:TXL-LMMNA along with ACMF leads to DNA damage as well as complete ablation of sensitive A2780^S and A2780-CisR cancerous tumor. This treatment ensures recovery and prolonged survival of tumor xenograft bearing mice as inferred by our investigation.

In vitro cytotoxicity measurement

The cytotoxicity of LMMNA, cisplatin (Sigma Aldrich), doxorubicin:paclitaxel (DOX:TXL) and DOX:TXL-LMMNA were assessed by Sulforhodamine-B assay for A2780^S and A2780-CisR cells. The cells were seeded into 96-well plates at 1 × 10^4 density per well overnight and incubated with defferent concentrations of LMMNA, cisplatin, DOX:TXL and DOX:TXL-LMMNA diluted in media for 24 h or 48 h. Cytotoxicity was assessed using Sulforhodamine-B (SRB, Sigma-Aldrich) assay as per manufacture's instruction and viability (%) was calculated using the following formula,

$$\% \text{ cell viability} = \frac{\text{absorbance of treated sample}}{\text{absorbance of control}} \times 100; \quad \ldots(3)$$

In vitro thermo-chemotherapy

For *in vitro* thermo-chemotherapy, 1 × 10^6 cells were seeded into 35 mm dish and treated with either DOX:TXL (40+30 µg/ml) or Cisplatin (5 µg/ml), LMMNA (1 mg/ml), or DOX:TXL-LMMNA (0.5 and 1 mg/ml) for 1 h. Simultaneously, another set of cells treated with LMMNA and DOX:TXL-LMMNA were kept under ACMF for 20 min at 376 Oe (250 kHz). Following this treatment cycle, all cells were incubated at 37 ˚C for 24 h, washed thrice with PBS and harvested by trypsinization. The percentage viability after different treatments was determined using trypan blue dye exclusion assay [20]. For quantification of apoptotic population, trypsinized cells were stained with Propidium Iodide (PI) as described earlier [18] and a minimum 10,000 events were recorded using flow cytometry (BD FACSCalibur) and analyzed by Motif software to determine the percentage of apoptotic population.

Fluorescent imaging of *in vivo* bio distribution of DOX:TXL-LMMNA particles

All animal experimentations were performed as per approval of the Institutional Animal Ethics Committee of Advanced Centre for Treatment, Research and Education in Cancer (ACTREC). Female BALB/c NUDE (6–8 weeks old) mice were used for bio distribution study of DOX:TXL-LMMNA. Utilizing the fluorescent properties of Doxorubicin entrapped into DOX:TXL-LMMNA biodistribution study was performed in real time for six time points (Day 0, Day 1, Day 2, Day 7, Day 30 and Day 60) (n=5 for each group) by *in vivo* fluorescent imaging with IVIS imaging system (see ESI Table S1). All these mice except the control ones were injected with 50 mg/kg of DOX:TXL-LMMNA (in 70 µl of sterile PBS) either by intra-peritoneal or intra-venous injections. The mice were anesthetized using isoflurane and whole body fluorescence spectra was acquired pre and post particle administration [21, 22]. Fluorescence spectra from each mice image was spectrally unmixed and analyzed using Live Imaging Software, 4.0. At the end of each imaging experiment, mice were sacrificed for organ specific iron content measurement.

ICP-AES, and magnetization properties of residual particles in organ

Iron quantity of LMMNA accumulated in different organs from bio distribution and thermo-chemotherapy studies was determined by ICP-AES and magnetization measurement. All the tissues were collected, fixed with 10% formaldehyde solution for overnight and were vacuum-dried for 2 days at 50 °C and then crushed to obtain powder. The mixed powder was used for magnetization measurements at room temperature using a superconducting quantum interference device (SQUID) magnetometer (MPMS). For ICP-AES analysis, powder samples were dissolved thoroughly in concentrated hydrochloric acid and filtered through filter paper to determine the iron concentration in different organs [23, 24].

TEM analysis of different organs

The vital organs harvested from control or treated mice were collected at different time points and fixed with 1 ml of 2.5% glutaraldehyde for 1 h at room temperature. The small portion of tissues were rinsed thrice with PBS and treated with 100 µl of 1% osmium tetroxide solution for 1 h and dehydrated with different ratios of alcohol. The tissues were then fixed in a 50:50 mixture of propylene oxide and resin overnight. Ultrathin sections were prepared from tissue embedded resin mold and placed on a copper grid for TEM analysis [22].

Table 1: Represent the level of "Fe" content in different organs pre and post administration of DOX:TXL-LMMNA at different time poionts.

Organs	Day 0	Day 1	Day 7	Day 60
Spleen	~ 0.1%	~ 16%	~ 17%	~ 0.4%
Lung	~ 1%	~ 12%	~ 13%	~ 0.9%

Bioluminescence imaging of A2780^S and A2780-CisR tumor xenografts

Animal care and euthanasia were performed with the approval from Institutional Animal Ethics Committee of ACTREC. Mice were implanted with 7 × 10^6 cells of either A2780^S or A2780-CisR stably expressing bi-fusion reporter (firefly luciferase-tandom tomato red (*fl2-tdt*)) and tumors were allowed to grow till 5-8 mm. For estimating anti-tumor activity of DOX:TXL-LMMNA nanoassembly, mice (n=15) were divided into three groups: I) untreated II) injected with DOX:TXL-LMMNA (50 mg/kg of DOX:TXL-LMMNA) (once intratumorally) without ACMF and III) injected with DOX:TXL-LMMNA and treated with ACMF (see ESI Table S2). For ACMF treatment, mice were anaesthetized with avertin (150 mg/kg mice weight) and subjected to ACMF at 376 Oe, 250 kHz (hyperthermia double dose: 1st dose at 0 h and 2nd dose at 24 h) by placing them into the 6 cm coil. The temperature of tumor surface was measured with an alcohol thermometer (Paico deluxe) at different time points. Whole body bioluminescence imaging of mice using IVIS-Spectrum optical imager was obtained after intra-peritoneal injection of 100 µl D-luciferin (0.4 mg/mouse) diluted in phosphate-buffered saline. Region of Interests (ROIs) were drawn over the tumors and quantified by using the Live Image (4.4) software. Bioluminescence signals were recorded as maximum (photons/s/cm^2/sr). The volume of the tumors and body weights were recorded and compared across the groups. The tumor volume was calculated using the following formula [24, 25]:

$$Tumor\ volume = \frac{1}{2}(length \times width^2) \quad \ldots(4)$$

After completion of imaging experiments, mice from all groups (group I, II and III) were sacrificed at Day 7 and organs, namely, the large intestine, small intestine, lung, liver, spleen, heart, kidney, stomach, brain, tumor, and normal skin were collected and preserved in 10% formaldehyde to determine the amount of "Fe". Toxicity was evaluated by measuring the total body weight and weights of all the organs before proceeding for preservation [23]. For the follow up study, mice with completely regressed tumors were kept for six months and monitored for physical appearance of tumor mass.

For the resistant tumor xenograft study, A2780-CisR cells were implanted at two sites per mouse and tumors were allowed to grow till 5-8 mm. A2780-CisR-tumor-bearing mice were divided into four major groups (n=5) according to treatment modality, that is, I) cisplatin (3.5 mg/kg), II) DOX:TXL (3.5 mg/kg), III) LMMNA and IV) DOX:TXL-LMMNA (see ESI Table S3). Each of these groups was treated with intra-tumoral injection of respective therapy regiment and tumor growth kinetics was measured by bioluminescence imaging and tumor volume.

Immunofluorescence studies and H&E staining

Immunofluorescence studies were performed as described earlier (Gaikwad et al. [19]). Briefly, cells seeded on coverslips were fixed with 4% paraformaldehyde, permeabilized with 0.025% Triton-X and probed with yH2.X antibody for overnight at 4 ˚C. Next day, after two hours of incubation with secondary antibody, cells were counterstained with DAPI and images were observed under Carl Zeiss, LSM 710 microscope. At least 50 cells were analysed from each group. Hematoxylin & eosin (H & E) staining was performed according to standard procedure on tissue sections.

Statistical analysis

Each experiment was carried out in triplicate at least three different times. The data are expressed as mean ± standard deviation (SD). The statistical analysis was determined by an unpaired two-tailed T-test using GraphPad Prism 6 software. The significant differences between the values are denoted as follows: $p < 0.05$ (denoted *), $p < 0.01$ (denoted **) and $p < 0.001$ (denoted ***).

3. Results and discussion

Characterization of DOX:TXL-LMMNA particles

Detailed characterisation and size distribution of MMNA and LMMNA particles were already reported in our earlier study [18]. Briefly, TEM images demostrated spherical structure of MMNA with a diameter of 73 nm which after coating (LMMNA) increased to 92 nm (as demonstrated in our pevious study), (see ESI Figure S1) [18]. The hydrodynamic diameter of LMMNA did not alter significantly (157 nm vs. 159 nm) when measured in PBS or serum-supplemented growth medium (DMEM) using dynamic light scattering (DLS) (see ESI Figure S2). This result indicated that LMMNA provide good suspension stability in PBS as well as in DMEM. A stable and consistant magnetic properties of these particles were also confirmed by VSM (evaluated in our previous report and data not shown) [18]. We also reported that DOX:TXL-LMMNA particles are able to release higher amount of DOX (~88%) and TXL (~53%) in the acidic media (pH 4.3) compared to ~28% of DOX and 26% of TXL at neutral condition (pH 7.4) over a period of 172 h. These DOX:TXL-LMMNA also show temperature dependent increased drug

discharge where ~23% of DOX and ~32% of TXL were released at 43 °C as compared to ~18% of DOX and ~21% of TXL at 37 °C [18]. For the current *in vivo* study, the loading efficiency of DOX and TXL was determined to be 81±2 and 60±3% and the loading capacity were 0.04±0.0004 and 0.03±0.0018 mg/mg at 5:2:2:2 ratio of LMNNA, respectively (ESI Figure S3).

Effect of combined thermo-chemotherapy *in vitro* on A2780^S cells

The cytotoxic effect of the combined thermo-chemotherapy was evaluated on A2780^S cells using dye exclusion assay as indicated in Figure 1. Administration of ACMF field decreased viability of A2780^S cells (86±2.57% to 48±0.41%) after LMMNA treatment (Figure 1A). Interestingly, dual drug loaded with DOX:TXL-LMMNA (0.5 mg/ml) nanoassembly demonstrated a significant decrease in viability (21.6±1%) compared to LMMNA+ACMF treatment (48±0.41%) ($p < 0.001$). Similarly, administration of higher dosage of DOX:TXL-LMMNA (1 mg/ml) showed further decrease in cell viability (6±0.3%) in these cells. These high doses of drug loaded particles were particularly chosen to mimic the *in vivo* dose condition where maximal magnetization was observed earlier [18]. DOX alone treatment (40 µg/ml) showed cellular viability of 34.5±4.5% compared to the control. Treatment of free DOX:TXL showed an increased cytotoxicity in dose dependent manner where cell viability decreased form 17±2.9% to 7.2±0.26% at a concentration of 35 and 70 µg/ml respectively. However, toxicity exerted by the free drugs were 5-7% more severe than the DOX:TXL-LMMNA particles. Both 35 and 70 µg/ml

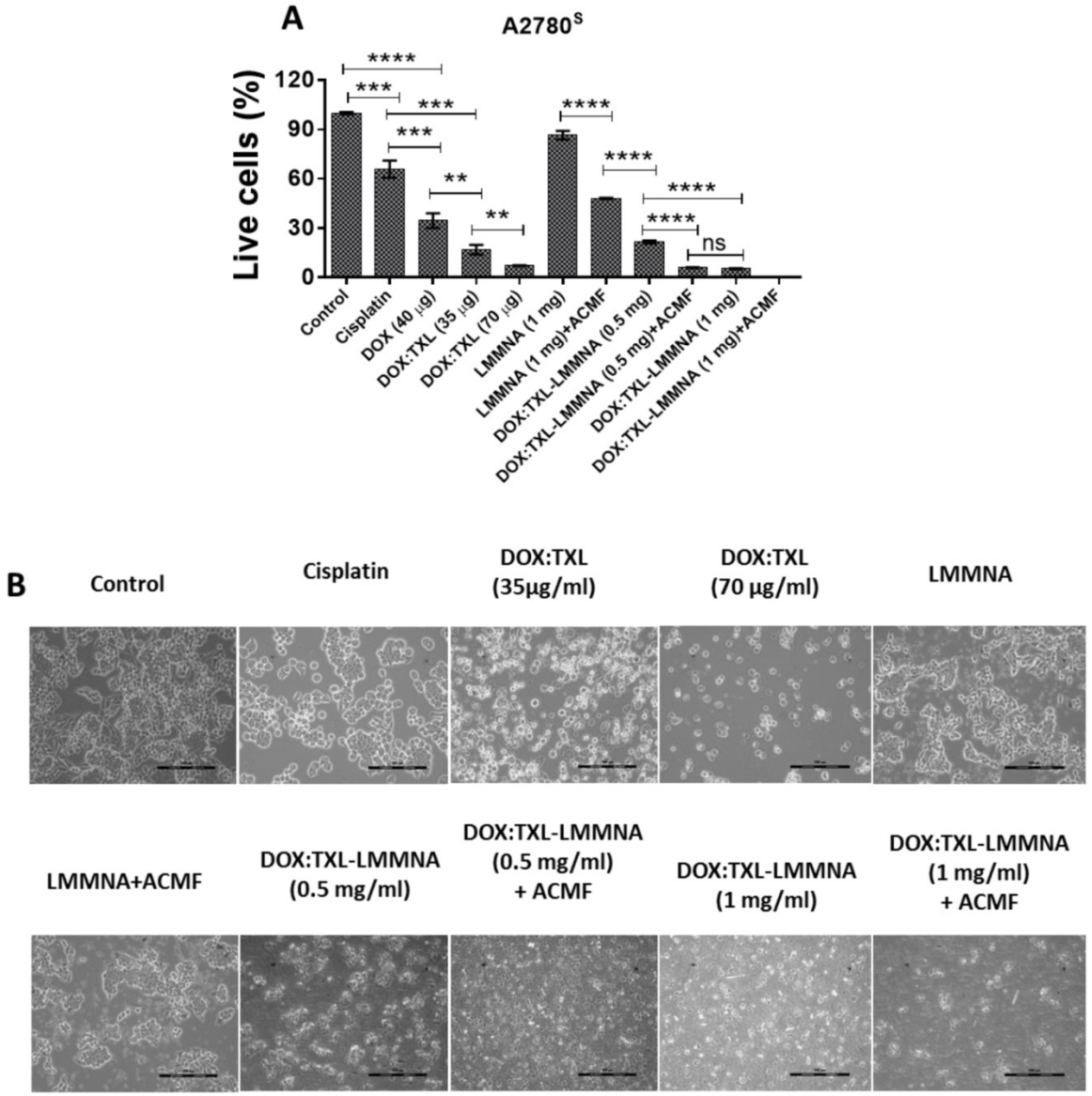

Figure 1. *In vitro* thermo-chemotherapy study on A2780^S cell line post 24 h of treatment. (A) Percent live cell count and (B) cellular morphology changes by optical microscopy after indicated treatment to A2780^S cells. Data expressed as mean ± SD (n=3). Significance is denoted as ** $p < 0.01$, *** $p < 0.001$ and **** $p < 0.0001$ and *ns* as no significance. Scale bar 100 µm.

concentration of free DOX:TXL correspond to drug loaded into 0.5 and 1 mg/ml of DOX:TXL-LMMNA respectively. ACMF administration to DOX:TXL-LMMNA (both at 0.5 and 1 mg/ml) further decreased viability from 21±1% to 6±0.3% and 5.4±0.3 to 0%, respectively. These observations indicate that hyperthermia induced by ACMF field improves efficacy of heat sensitive DOX:TXL-LMMNA in $A2780^S$ cells. This improved drug efficacy can be due to enhanced uptake and accumulation of intracellular DOX:TXL from temperature induced hyper-permeability of the cell membrane and DNA damage [8, 13, 14, 26, 27]. Additionally, microscopic examination revealed drastic changes in cellular morphology when $A2780^S$ cells were treated with DOX:TXL-LMMNA+ACMF compared to either treatment alone (Figure 1B). The rounded appearance of the cells subjected to all treatments including DOX:TXL, LMMNA+ACMF, DOX:TXL-LMMNA with/without ACMF (at 0.5-1 mg/ml) were indicative of cell apoptosis. Further, apoptosis induction in these cells were quantified using PI staining. Cells treated with LMMNA and DOX:TXL-LMMNA in presence of ACMF showed higher percentage of apoptotic cells (13% and 38%) compared to absence of ACMF for both LMMNA (~0.45%) and DOX:TXL-LMMNA (~21%) treatment (ESI page 7).

In vivo bio distribution of DOX:TXL-LMMNA

In order to evaluate the toxicity of DOX:TXL-LMMNA *in vivo*, overall growth and tissue bio distribution were investigated in NUDE mice. DOX:TXL-conjugated LMMNA offers an added advantage of fluorescence property of doxorubicin which can be imaged in *in vivo* [14, 28] and therefore both non-invasive fluorescence imaging and ICP-AES analysis of tissue homogenates were utilized to monitor the kinetics of distribution and retention properties of these particles. As shown in Figure 2A, higher fluorescence signal demonstrated the presence of non-targeted DOX:TXL-LMMNA mainly in the abdominal area immediately after intra-peritoneal or intra-venous injection. On second day, fluorescence signal was observed from all over the body in the mice which were subjected to intravenous injection. In contrast, intraperitoneal injection of the particles showed a localized (abdominal) signal indicating a lower/slower distribution rate. The signals remained stabilized for 7 days and decreased with time and completely disappeared by Day 60. This indicates that DOX:TXL-LMMNA are cleared from NUDE mice over a period of 60 days.

The organ-specific retention of DOX:TXL-LMMNA was estimated by measuring 'Fe' content in different organs through ICP-AES analysis. Corroborating to our non-invasive fluorescence bio distribution studies, increased 'Fe' level was observed in all organs except skin and brain tissue post 24 h DOX:TXL-LMMNA administration (Figure 2(B & C)). Interestingly, intra-venous administration showed relatively higher 'Fe' content in spleen, stomach and heart compared to intra-peritoneal administration of DOX:TXL-LMMNA (Figure 2C). No significant difference was observed in iron retention for other organs based on route of administration. Iron content in all tissues remained stable till Day 7 and then decreased over time for both intra-venous and intra-peritoneal mode of administration. This data was also corroborated with magnetization properties of these particles measured from each organ. The highest magnetization value of all organs based on the amount of "Fe" concentration was obtained with M-H loop (see ESI Figure S4). As shown in Figure 2D, the highest magnetization values were obtained from the large intestine (0.03±0.004 emu/g), lung (0.03±0.004 emu/g), spleen (0.06±0.011 emu/g), liver (0.012±0.001 emu/g) and kidney (0.03±0.002 emu/g) till Day 7, which decreased gradually over a period of 60 days indicating both hepatobiliary and renal excretion mode of clearance. The accumulation of "Fe" in the small intestine, kidney, stomach, and the heart were found to be minimal at Day 60. As shown in Figure 2E, no significant differences were observed in the organ weight profile between control and DOX:TXL-LMMNA treated mice except for large intestine and the mice did not show any discomfort or any overt clinical signs of toxicity.

In vivo disassembly of DOX:TXL-LMMNA in different organs

Spontaneous disassembly of DOX:TXL-LMMNA is required to avoid toxicity and clearance from body. Since our bio-distribution data indicated maximal accumulation of DOX:TXL-LMMNA in spleen and lung, TEM analysis was performed to confirm particle integrity. As shown in Figure 3B & C, intact DOX:TXL-LMMNA were found at Day 1. By Day 7 (Figure 3D & E), most of these assemblies were disintegrated and very few of them retained their original morphology. In addition, localization of nanoassemblies inside the tissue by Day 7 can also be confirmed in the ESI Figure S5. Further these particles were cleared out from the spleen and the lung as TEM analysis did not detect presence of these particles by Day 60 (Figure 3F). As shown in Table 1, percent weight accumulation of 'Fe' gradually decreased over a period of 60 days in the spleen and lung tissues. Thus we believe that these nanoassemblies undergo spontaneous degradation which facilitates their clearance from the organs over time.

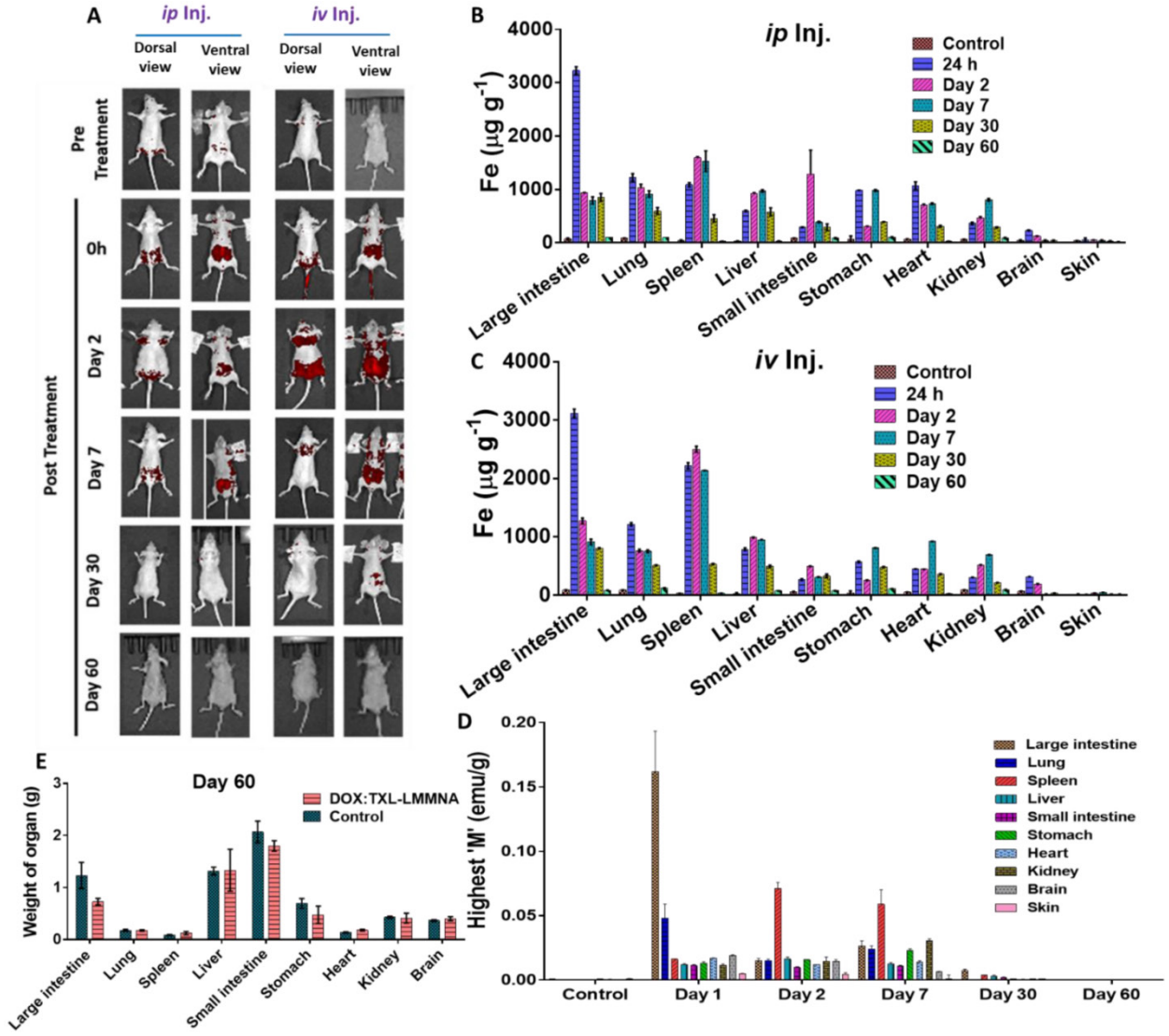

Figure 2. *In vivo* bio distribution and clearance of DOX:TXL-LMMNA post intra-venous (iv) and intra-peritoneal (ip) administration in female NUDE mice (n=5). (A) Representative whole body fluorescence imaging of DOX:TXL-LMMNA bio distribution over a period of 2 months. (Red color represents the spectrally unmixed fluorescence signal of the DOX at 580 nm). A gradual reduction in the fluorescence intensity indicates disintegration and excretion of the nanoparticles by the hepatobiliary route. (B & C) Iron content 'Fe' (μg/g) of each organ tissue post DOX:TXL-LMMNA administration as determined by ICP-AES analysis at various time points. (D) Highest magnetization values of vital organ tissues at various time points and (E) Comparison between organ tissue weights of the treated and untreated mice at Day 60.

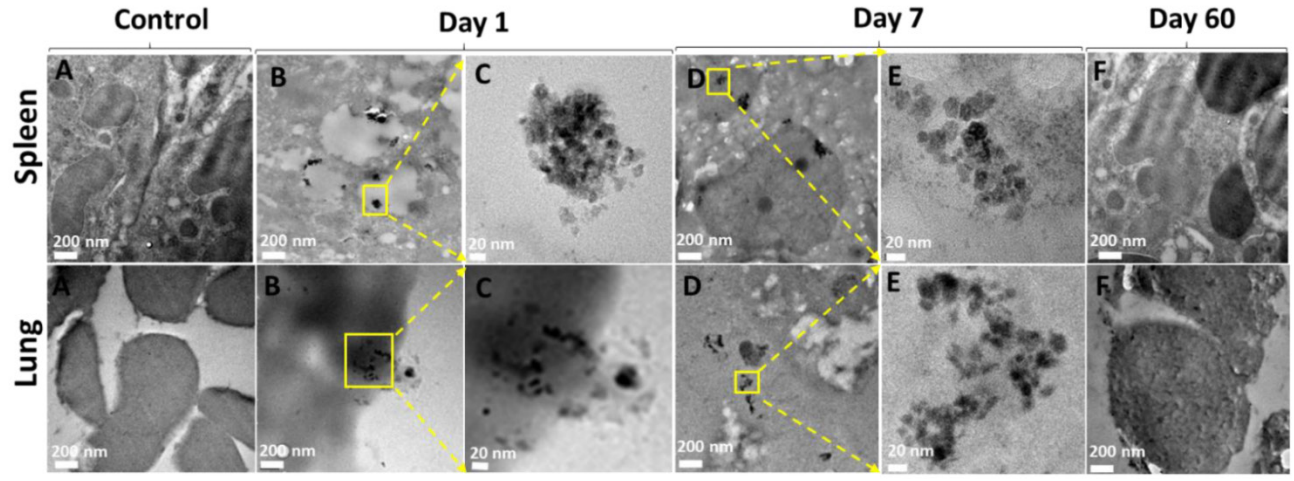

Figure 3. TEM images of uptake and accumulation of nanoparticles in spleen and lung tissues after Day 1, Day 7 and Day 60 treatment. Column (A) untreated spleen and lung tissue, column (B) both tissues show morphology with accumulation of LMMNA after Day 1, column (C) magnified image of the area indicated by the yellow box in column (B), column (D) shows morphology with accumulation of LMMNA after Day 1, column (E) magnified image of column (D) marked as yellow box, showing the nanoassemblies into tissue at Day 7, column (F) shows tissues morphology at Day 60 which is similar to the untreated control column.

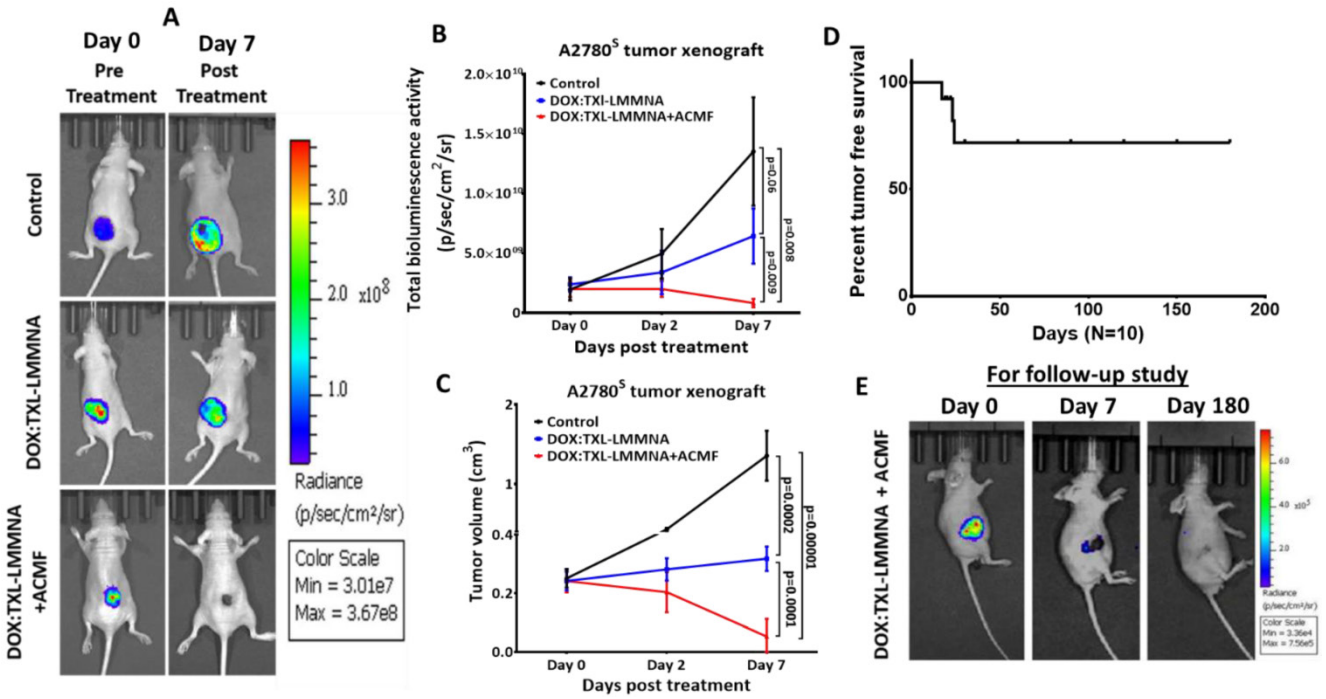

Figure 4. *In vivo* combined therapy using 1 mg of DOX:TXL-LMMNA in mice bearing A2780^S tumor xenografts (n=5). Tumor regression was monitored by bioluminescence imaging in the absence/presence of ACMF at 376 Oe, 250 kHz frequency on the A2780^S tumor xenografts after intratumoral injections. (A) Representative bioluminescence images of *in vivo* combined therapy evaluation against A2780^S tumor xenografts. (B) Graphical quantification of bioluminescence signal showed significant decrease in bioluminescence of tumor post DOX:TXL-LMMNA compare to control by Day 7 on A2780^S tumor xenografts (significance difference indicates as p= 0.06, p= 0.009 and p= 0.008). (C) Tumor volume measurement of A2780^S tumor xenografts showed decrease in tumor volume post DOX:TXL-LMMNA with and without treatment of ACMF at different time points (significance difference indicates as p= 0.0002, p= 0.0001 and p= 0.00001). (D) Kaplan-Meier survival curve for the tumor free survival of mice treated with DOX:TXL-LMMNA+ACMF combined therapy (A2780^S tumor). (E) Representative bioluminescence imaging for 6 month follow-up study of DOX:TXL-LMMNA+ACMF treatment on mice bearing A2780^S tumor xenografts.

In vivo therapeutic efficacy of DOX:TXL-LMMNA on A2780 ^{S} tumor xenografts

To study the anticancer activity of DOX:TXL-LMMNA in combination with ACMF, mice carrying A2780^S tumor xenografts were injected with the particles and subjected to ACMF treatment. Administration of DOX:TXL-LMMNA increased the temperature of the tumor surface up to 41±0.25 °C within 15 min and remained constant over time (ESI Figure S6). For group III animals (as mentioned in method section), ACMF was given twice for 20 min within 48 h after single dose of DOX:TXL-LMMNA injection. Our study revealed a significant reduction in tumor bioluminescence signal for group III by 0.34 ± 0.18 fold change (from $2.26\times10^9 \pm 2.39\times10^9$ to $7.7\times10^8 \pm 1.3\times10^9$ p/sec/cm^2/sr) as compared to group I (from $3.46\times10^9 \pm 3.37\times10^9$ to $3.13\times10^{10} \pm 3.37\times10^{10}$ p/sec/cm^2/sr, 8.7 ± 1.25 fold change) (p= 0.002) or group II (from $4.65\times10^9 \pm 5.17\times10^9$ to $2.46\times10^{10} \pm 4.1 \times 10^{10}$ p/sec/cm^2/sr, 4.15±2.61 fold change) (p= 0.0068) animals (Figure 4A & B). This was also corroborated with tumor volume where in group III, all animals except one showed complete tumor regression (0.2±0.21 fold change) compared to the control (group I) and only DOX:TXL-LMMNA treated animals (group II) showed a fold change of 5.4±0.7 and 1.32±0.03 in tumor volume respectively (Figure 4C).

To monitor long term potential of these particles, mice (n=10) showing complete tumor regression were followed upto 6 months. As shown in Figure 4D, only 3 out of 10 mice showed relapse while the rest did not show any palpable tumors. Bio luminescence imaging of these mice (with no relapse) after 6 months also did not show any signal indicating complete absence of viable tumor cells (Figure 4E). All these data indicate a remarkable potential of these magnetic nanoparticles containing very low doses of drugs to effectively kill tumor cells. The possible mechanism involves hyperthermia induced enhanced permeability of the cell membrane through ACMF, and higher accumulation of drugs in the tumor site [8, 13, 14].

DOX:TXL-LMMNA particle retention in the different organs post thermo-chemotherapy

In order to understand the effect of ACMF on the organ specific retention of DOX:TXL-LMMNA nanoassembly, iron content of each organ was estimated using ICP-AES analysis at Day 7. As shown in Figure 5A, no significant alteration in organ specific accumulation was observed post application of ACMF except for tumor tissue. Low level 'Fe' accumulation in tumor tissues explains disassembly

of these nanoparticles after ACMF exposure, suggesting site specific drug release at the tumor site for the DOX:TXL-LMMNA+ACMF treatment group, in comparison to the DOX:TXL-LMMNA treatment group (Figure 5A). As an additional validation for disassembly of DOX:TXL-LMMNA in tumors, assessment of magnetization properties and fluorescence imaging were performed in absence/presence of ACMF at the end of Day 7. Higher magnetization values were observed in tumors treated with DOX:TXL-LMMNA (0.4±0.04 emu/g) as compared to DOX:TXL-LMMNA+ACMF (0.02±0.003 emu/g) treatment (ESI Figure S7A). Fluorescence signal in DOX:TXL-LMMNA+ACMF treated mice completely disappeared in comparison to DOX:TXL-LMMNA treated mice at Day 7 (ESI Figure S7B). These results confirm occurrence of rapid disintegration of nanoassemblies under the action of ACMF. For both DOX:TXL-LMMNA and DOX:TXL-LMMNA+ACMF conditions, higher accumulation of "Fe" was observed in lung, spleen and liver compared to other organs at Day 7. In order to understand the toxic effects of these particles, all organs collected from the three groups of animals were weighed.

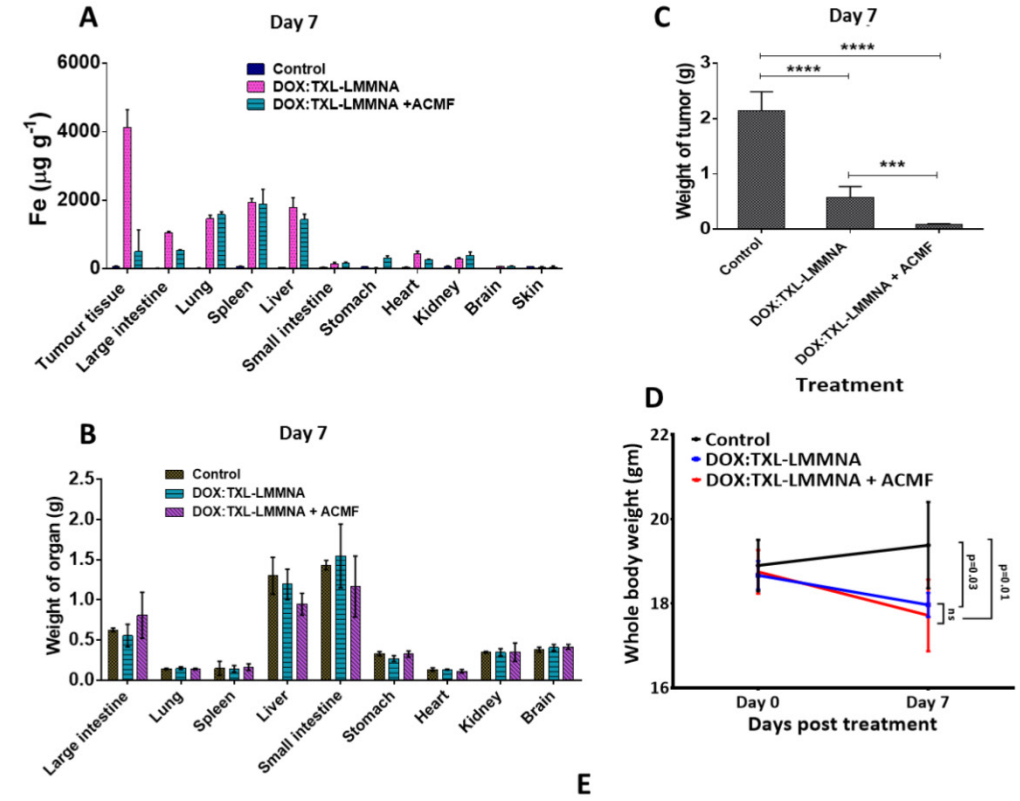

Figure 5. *In vivo* cytotoxicity studies using 1 mg of DOX:TXL-LMMNA in the absence/presence of ACMF at Day 7 in the A2780^S sensitive tumor xenograft bearing NUDE mice. (A) Quantitative estimation of the 'Fe' from different organs of the mice at Day 7. (B) Measurement of weight of all organs after treatment at Day 7. (C) Graphical representation of the tumor weight showed decreases tumor weight after combined therapy at Day 7. (D) Whole body weight of mice treated with DOX:TXL-LMMNA decreases due regression of tumor post therapy. (Significance difference indicates as p= 0.03, p= 0.01 and *ns* as no significance). (E) Histological analysis of tumor tissue using DOX:TXL-LMMNA in the absence/presence of ACMF. All sections stained with Hematoxylin & Eosin (H & E). DOX:TXL-LMMNA treated tumor section shows necrotic lesion which increases in the tumor tissue treated with DOX:TXL-LMMNA+ACMF. Yellow star indicate necrotic cells whereas red arrow indicate immune-associated cells in the tumor sections. Significance is denoted as *** $p < 0.001$ and **** $p < 0.0001$ and *ns* as no significance.

As shown in Figure 5B, no significant difference was observed in the organ weights among each group. A significant decrease in the total tumor weight from Day 0 to Day 7 was observed for group II-DOX:TXL-LMMNA (0.6±0.2 fold) animals compared to the control group (increased by 2±0.4 fold) (Figure 5C). The slight increase in total body weight in control group from Day 0 (19±1)g to Day 7 (20±1)g was possibly resulted from increased tumor volume. In contrast, in mice treated with DOX:TXL-LMMNA and DOX:TXL-LMMNA+ACMF, slight decline in body weights were observed (18±0.5)g and (17±1)g at Day 7 in comparison (~(19±0.6)g and (18±1)g) at Day 0 (Figure 5D). This data was also corroborated with histopathological analysis of H & E stained tumor tissue sections from control mice and mice treated with DOX:TXL-LMMNA and DOX:TXL-LMMNA+ACMF. As shown in Figure 5E, the control tumor tissue section did not show any noticeable inflammatory or necrotic lesion. However, the DOX:TXL-LMMNA treated tumor tissue sections showed various necrosis lesions (shown with yellow star), degree of which increased post ACMF treatment. Interestingly, tumor treated with DOX:TXL-LMMNA showed increased immune-associated cells indicating inflammatory response (shown with red arrow in Figure 5E). This inflammatory response escalated after ACMF application in combination with DOX:TXL-LMMNA treatment. Thus altogether our data suggest that this thermo-chemo combined therapy with drug loaded smart nanoparticle is able to exert complete regression of tumors without any toxic effect on the vital organs of mice.

In vitro cytotoxicity assay of DOX:TXL-LMMNA on cisplatin resistant cell line A2780-CisR

Development of resistance towards the first line chemotherapy (platinum and taxol based drugs) is a serious problem for epithelial ovarian cancer patients and no alternate therapy has shown success in the relapse setting. *In vitro* cytotoxicity of DOX:TXL-LMMNA was previously reported with various sensitive cell lines across different cancer types (HeLa, MCF-7 and HepG2 cells) respectively. The viability of HeLa, MCF-7 and HepG2 cells were observed to be ~41±1%, ~40±1% and ~44±2% respectively [18]. In order to evaluate the effect of these magnetic nanoparticles on cisplatin resistant (A2780-CisR) ovarian cancer cell line, both $A2780^S$ and A2780-CisR cells were treated with LMMNA, cisplatin, doxorubicin+paclitaxel (DOX:TXL) and DOX:TXL-LMMNA and cytotoxicity were estimated post 24 and 48 h of treatment. While the $A2780^S$ cells exhibited ~69±1% and ~38±4% viability at 24 and 48 h respectively (Figure 6A & C), A2780-CisR cells demonstrated more than 90% viability post 24 and 48 h of treatment, (Figure 6B & D) when treated with 5 μg/ml of cisplatin. However, both these cells showed 90% viability when incubated with 1 mg/ml of LMMNA upto 48 h indicating good biocompatibility. This again suggested the non-toxic nature of LMMNA particles. Further, to determine the anticancer effect of DOX:TXL-LMMNA, 1 mg/ml (correspond to 40 and 30 μg/ml concentration of DOX and TXL respectively) particles and similar amount of free drugs were added to $A2780^S$ and A2780-CisR cells for 24 and 48 h. In presence of particles, both $A2780^S$ and A2780-CisR cells exhibited cell viability upto 9±0.5% at 24 h and 4±0.4% at 48 h and 12±2% at 24 h and 8±1% at 48 h respectively. Though A2780-CisR cells are resistant towards cisplatin, they showed sensitivity to free DOX:TXL drugs with 37±1% and 30±2% viability (24 h and 48 h respectively) compared to 12.2±1.7% and 8.6±1.2% viability in sensitive cells. Interestingly, in presence of DOX:TXL-LMMNA particles, the A2780-CisR cells exhibited significantly higher cell death (36%) compared to the free DOX:TXL treatment. Altered pH gradient and increased lysosomal compartmentalization of chemotherapeutic agents are known to induce drug resistance in cancer cells [31-34]. The drug loaded nanoassemblies have shown to accumulate in the lysosomal compartment of cells after endocytosis [18]. Thus this hypersenstivity of drug resistant cells towards the nanoparticles might be due to highly acidic lysosomal milieu which is a known feature of drug resistant cells.

Effect of combined thermo-chemotherapy on cisplatin resistant A2780-CisR cells

Next the cytotoxic effect of combined thermo-chemotherapy with 0.5 and 1 mg/ml concentrations of DOX:TXL-LMMNA was evaluated in A2780-CisR cells for 24 h. The viability of resistant cells significantly reduced from 87±3.2 (treated with 1 mg/ml of LMMNA in absence of ACMF) to 50±3.4% ($p < 0.001$) after LMMNA+ACMF treatment (Figure 7A). Further, we observed that the viability was significantly decreased in a concentration-dependent manner of DOX:TXL-LMMNA (0.5 and 1 mg/ml) from 21 to 4.3% ($p < 0.01$) in the absence of ACMF. Administration of free DOX:TXL (at a concentration of 35 and 70 μg/ml) treatment showed that the cell viability decreased to 56.6±3.3% and 33±4% ($p < 0.01$) respectively, while DOX alone treatment at concentration of 40 μg/ml showed 69.1±4.3% cell viability. However, this sensitizing effect was observed in case of free DOX alone and DOX:TXL treatment and not with cisplatin (at 70 μg/ml)

treatment (87±2.3%) in A2780-CisR cells. Interestingly, when ACMF (for 20 min at 376 Oe, 250 kHz) was applied to cells treated with DOX:TXL-LMMNA+ ACMF (0.5 mg/ml) a significant reduction in viability (4.7±1.5%) was observed compared to only DOX:TXL-LMMNA treatment (21±4.2%) ($p < 0.01$). Similarly, ACMF application to cells incubated with 1 mg/ml of DOX:TXL-LMMNA decreased viability from 4.3±3.8% to 0% respectively. These results suggested that hyperthermia treatment with heat sensitive DOX:TXL-LMMNA enhanced the cytotoxic effect in A2780-CisR cells. More interestingly, the combined hyperthermia and chemotherapy can enhance the DNA damage and destroy the cell membrane in A2780-CisR and A2780^S cells [18]. Significant morphological changes of cells occur when A2780-CisR was treated with DOX:TXL-LMMNA+ ACMF compared to either treatment alone as shown in Figure 7B. Administration of DOX:TXL, LMMNA+ACMF, DOX:TXL-LMMNA with/without ACMF (at 0.5-1 mg/ml) showed the typical round morphology of apoptotic cells. Further, cells undergoing apoptosis were quantified using PI staining post respective treatments (see ESI Figure S8). Similar to A2780^S cells, A2780-CisR cells also showed higher apoptotic population in presence of ACMF after treatment with LMMNA or DOX:TXL-LMMNA (11% and 33%, respectively) compared to LMMNA or DOX:TXL-LMMNA treatment in absence of ACMF (0.2% and 20% respectively).

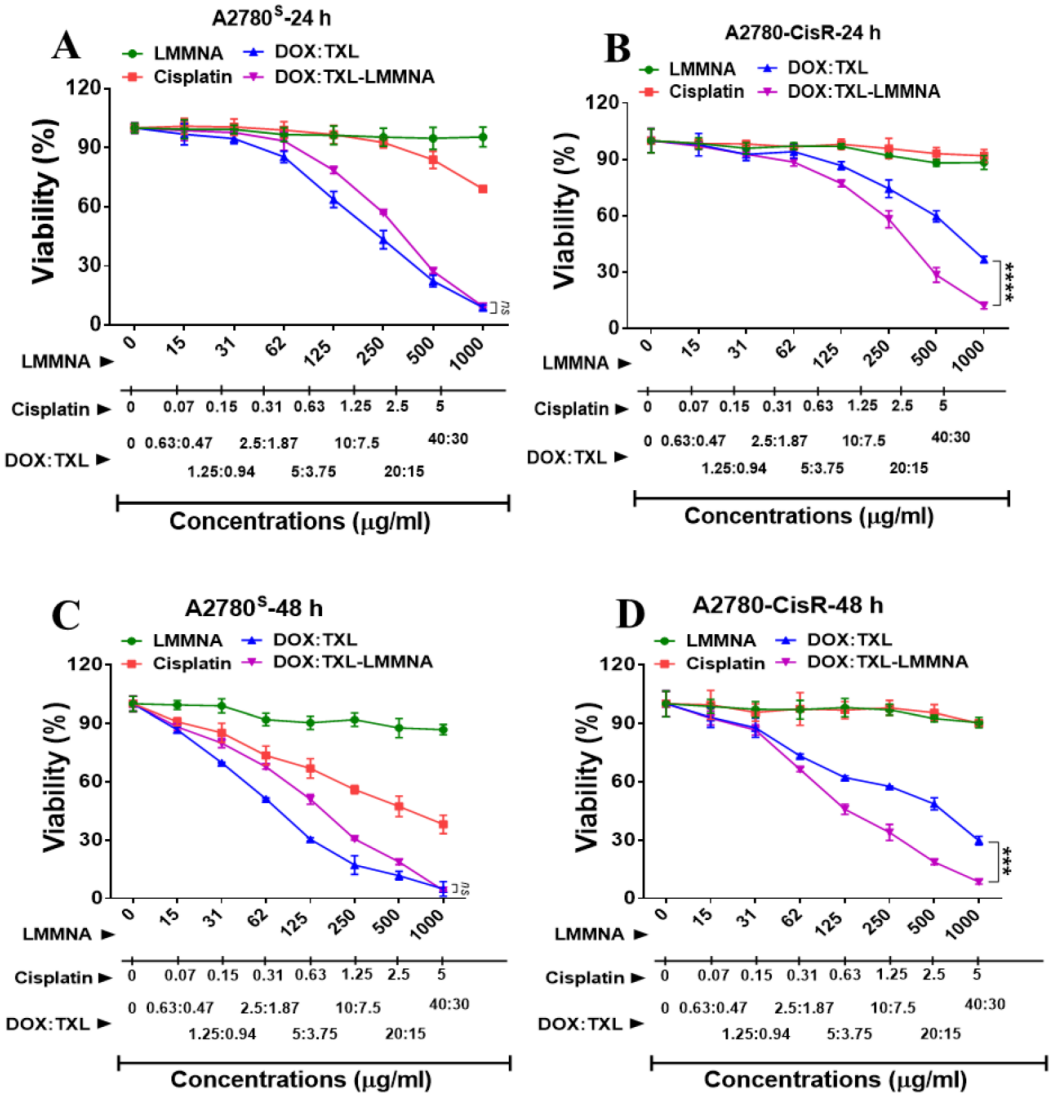

Figure 6. Time dependent *in vitro* cytotoxicity effect of LMMNA, free cisplatin, free DOX:TXL and DOX:TXL-LMMNA upto 1 mg/ml with different drug contents (A & B) at 24 h and (C & D) at 48 h on A2780^S and A2780-CisR cells. Data expressed as mean ± SD (n=3). Significance is denoted as *** $p < 0.001$ and **** $p < 0.0001$ and *ns* as no significance.

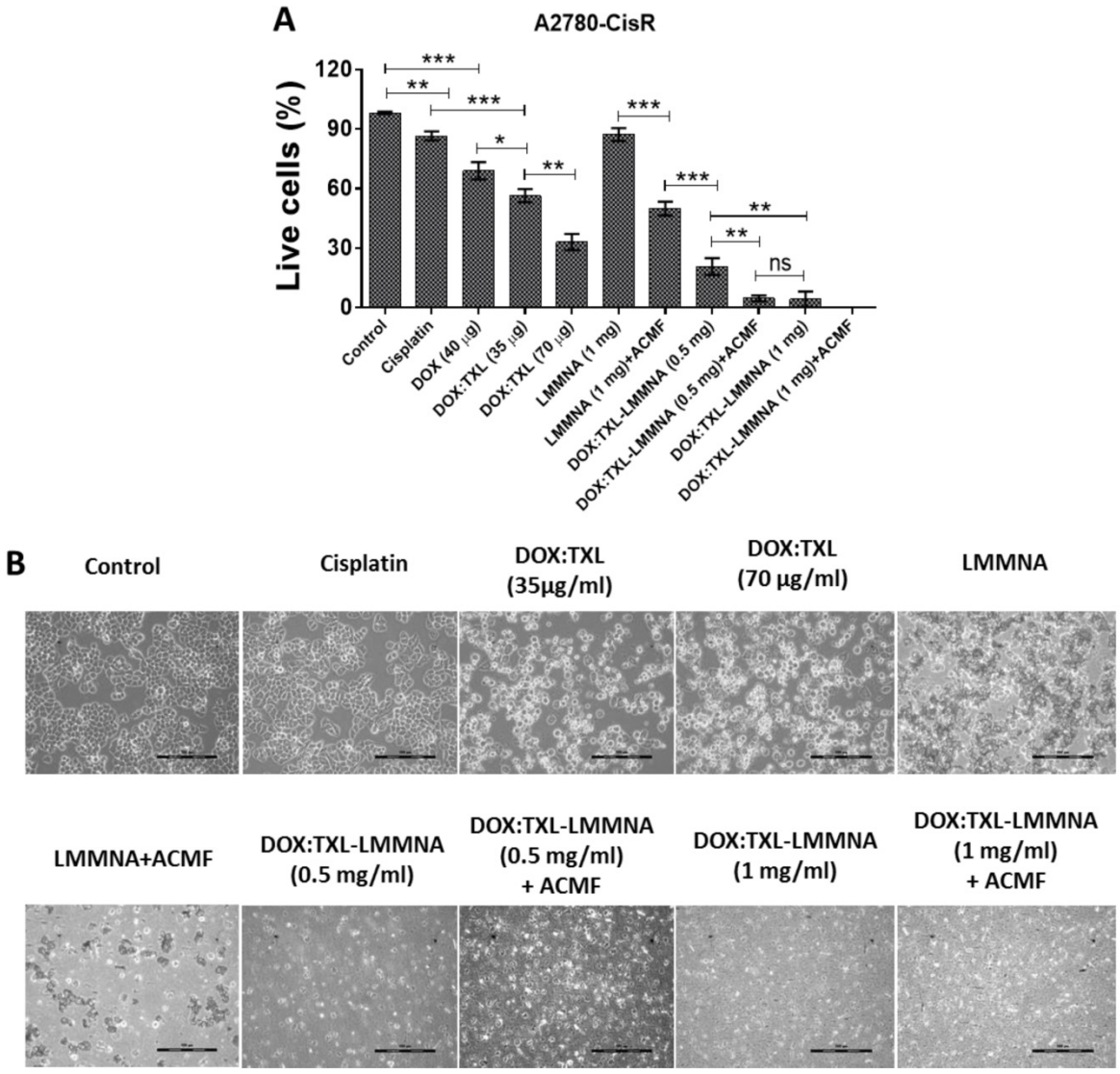

Figure 7. *In vitro* thermo-chemotherapy study on A2780-CisR cell line at 24 h. (A & B) efficiency of live cells after treatment and (C) optical microscopy images for morphological study. Data expressed as mean ± SD (n=3). Significance is denoted as ** $p < 0.01$ and *** $p < 0.001$ and *ns* as no significance. Scale bar 100 μm.

Efficacy of DOX:TXL-LMMNA with hyperthermia against cisplatin resistant A2780-CisR tumor xenografts

To understand the efficacy of thermo-chemotherapy *in vivo* on drug resistant tumors, 5 × 10^6 of A2780-CisR-cells were implanted either on two shoulders or shoulder and flank region of NUDE mice. All mice from each group were exposed to ACMF under the same conditions which have been previously described and imaged by injecting D-luciferin. Representative images of tumor regression evaluated using bioluminescence imaging are shown in Figure 8A. As shown in Figure 8B, in group IV mice (DOX:TXL-LMMNA+ACMF treated), tumor bioluminescence signal was decreased by 0.22±0.18 fold (from 2.2×10^7 ± 1.9×10^7 to 4.9×10^6 ± 5.2×10^6 p/sec/cm²/sr) post hyperthermia treatment. Resistant tumor treated with cisplatin or DOX:TXL alone showed increased bioluminescence activity from 2.1×10^7 ± 1.2×10^7 to 5.5×10^7 ± 3.03×10^7 p/sec/cm²/sr (3.7±1.96 fold change) and from 2.1×10^7 ± 1.7×10^7 to 6.7×10^7 ± 1.6×10^7 p/sec/cm²/sr (fold change by 4.79±3.27) respectively (Figure 8B). The increase in tumor signal by DOX:TXL is contrary to our *in vitro* data and occurred due to lower doses than the optimal one to show any effect in *in vivo* condition [34-37]. Resistant tumor on treatment with only LMMNA particles followed by hyperthermia showed minor change in bioluminescence activity (from 1.8×10^7 ± 9.8×10^6 to 1.5×10^7 ± 1.1×10^7 p/sec/cm²/sr (0.8±0.3 fold change) indicating cytostatic effect of these particles in combination with hyperthermia. Interestingly, the bioluminescence signal significantly ($p = 0.016$) decreased in A2780-CisR tumor as compared to $A2780^S$ tumor xenograft undergoing

similar treatment of DOX:TXL-LMMNA+ACMF (ESI Figure S9A).

The imaging results were also corroborated with tumor volume data where cisplatin and DOX:TXL treated tumor showed increased tumor mass by 2.18±0.49 and 3.52±1.3 fold respectively. Interestingly, LMMNA treated tumors demonstrated slight decrease in volume (0.65±0.2 fold change) whereas DOX:TXL-LMMNA+ACMF showed around 80% regression of tumor (0.22±0.18 fold change) volume (Figure 8C). DOX:TXL-LMMNA+ACMF treated resistant tumor showed significant ($p = 0.04$) decrease in tumor volume as compared to sensitive tumor as shown in ESI Figure S9B. To understand the effect of hyperthermia alone, we treated A2780-CisR cells with DOX:TXL in absence and presence of hyperthermia (incubated at 42 °C to mimic hyperthermia effect) and processed for γH2.X foci formation analysis as a marker of DNA damage at various time intervals (Figure 8D). As shown in Figure 8E, cells incubated at 37 °C showed highest mean fluorescence intensity of foci formation at 12 h which decreased by 24 h. This indicates that the DOX:TXL treatment is most effective till 12 h at 37 °C. Interestingly, cells incubated at 42 °C showed slightly lesser foci formation at 12 h which increased by 24 h. This indicated that hyperthermia (42°C) enhances the efficacy and duration of DOX:TXL treatment.

Again minimal change in body weights of mice were observed for to cisplatin (17±1)g, DOX:TXL+ACMF (18±2)g, LMMNA+ACMF (18±1)g and for DOX:TXL-LMMNA+ACMF (18±1)g treatment groups at Day 7 in comparison to Day 0 (19±1), (19±1), (19±1), and (20±1)g, respectively (Figure 8F). All together our data indicate that these novel nanoassemblies developed in this study have the potential to exert maximum cytotoxicity with low drug concentration without affecting the mouse physiology when induced by hyperthermia. Intriguingly, we have found that this cytotoxic effect is more pronounced in drug resistant cells/tumors.

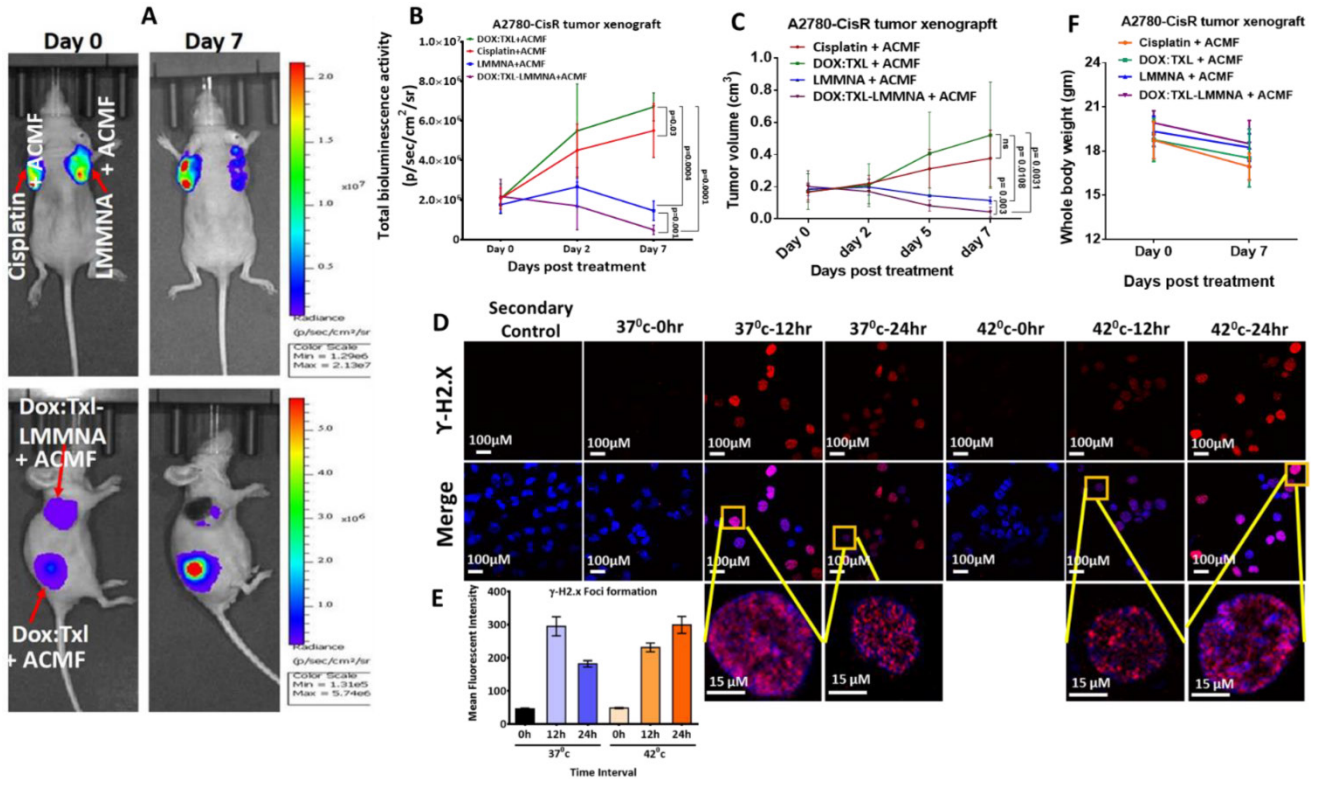

Figure 8. *In vivo* combined therapy using 1 mg of DOX:TXL-LMMNA in A2780-CisR tumor xenografts NUDE mice (n=5). Tumor regression study monitored by bioluminescence imaging in the absence/presence of ACMF at 376 Oe, 250 kHz frequency on the A2780-CisR tumor xenografts after intratumoral injections. (A) Representative bioluminescence images of A2780-CisR tumor xenografts after intratumoral injections of free cisplatin (3.5 mg/kg), DOX:TXL+ACMF (2:1.5 mg/kg), LMMNA+ACMF (50 mg/kg) and DOX:TXL-LMMNA+ACMF (2:1.5:50 mg/kg). (B) Quantitative assessment of bioluminescence signal showed significant decrease in bioluminescence signal of A2780-CisR tumor xenografts post combined therapy ($p= 0.03$, $p= 0.001$, $p= 0.0004$ and $p= 0.0001$). (C) Graphical representation of the tumor volume for A2780-CisR tumor xenografts showed decreases tumor volume post combined therapy ($p= 0.003$, $p= 0.0108$, $p= 0.0031$ and *ns* as no significance). (D & E) Effect of hyperthermia on drug efficacy assessed by γH2.X foci formation assay in A2780-CisR cancer cells. Hyperthermia increases the efficacy drug leads to increased γH2.X foci formation at 42 °C compare to 37 °C. (E) Graphical quantitation of γH2.X foci after each treatment. (F) Whole body weight measurement of mice bearing A2780-CisR tumor xenograft after each treatments at Day 0 and Day 7.

Conclusion

In summary, we have successfully developed a novel pH and thermo liable lipid-coated mesoporous magnetic nanoassembly for dual drug delivery and hyperthermia applications. This fomulation was optimized for combined hyperthermia and chemotherapy. The therapeutic efficacy was evaluated both *in vtro* and *in vivo* in cisplatin resistant and cisplatin sensitive ovarian cancer model ($A2780^S$ and A2780-CisR tumor xenograft animals) using molecular imaging techniques. The enhanced cytotoxic effect of DOX:TXL-LMMNA under ACMF resulted in higher cell death than treatment with only DOX:TXL-LMMNA on $A2780^S$ and A2780-CisR cells and tumors without any adverse effect on body physiology. The dual drug-delivery system is found to be effective and exhibits optimal therapeutic efficacy and complete tumor ablation at low concentrations, *in vivo*. Most importantly we found that the effect of these particles is more pronounced in drug resistant cells and tumors probably due to its inherent lysosomal acidic environment. Thus these novel stimuli sensitive nanoassemblies hold great promise for therapy of resistant malignancies and may be translated to clinics in near future. However, the non-targeted nature of these particles still pose limitation for ultimate application hence further improvement towards targeted delivery are under investigation.

Supplementary Material

Supplementary tables and figures.
http://www.thno.org/v06p1557s1.pdf

Acknowledgments

The authors would like to acknowledge ACTREC for the animal facility. BT acknowledges CSIR for fellowship. This study was partially funded by DBT (BT/PR8052/MED/32/298/2013) to PR. The authors thank the Nanomission of Department of Science and Technology (DST) and Nanotechnology Division: Department of Electronics and Information Technology (Deity), Government of India for financial support. We are also thankful to the Centre for Research in Nanotechnology and Science (CRNTS), I. I. T. Bombay and Dr. Bharat Rekhi for analyzing our histological tumor sections.

Abbreviations

ACMF, AC magnetic field; Chol., cholesterol; CisR, cisplatin resistant; DOX, doxorubicin hydrochloride; DMEM, Dulbecco's Modified Eagle's Medium; DPPC, 1,2-dipalmitoyl-sn-glycero-3-phosphocholine; $DSPE\text{-}PEG_{2000}$, 1,2-distearoyl-sn-glycero-3-phosphoethanolamine-N-[amino (polyethyl ene glycol)-2000]; EPR, enhances cellular permeability and retention effects; *fl2-tdt*, firefly luciferase-tandom tomato red; (H & E), Hematoxylin & eosin; ICP-AES, Inductively coupled plasma atomic emission spectroscopy; LMMNA, thin lipid layer with mesoporous magnetite nanoassemblies; MMNA, mesoporous magnetite nanoassemblies; ROIs, Region of Interests; SRB, Sulforhodamine-B; TEM, transmission electron microscopy; TXL, paclitaxel.

Competing Interests

The authors have declared that no competing interest exists.

References

1. Zafar S, Negi LM, Verma AK, Kumar V, Tyagi A, Singh P, et al. Sterically stabilized polymeric nanoparticles with a combinatorial approach for multi drug resistant cancer: *in vitro* and *in vivo* investigations. Int J Pharm. 2014; 477: 454-68.
2. He Q, Gao Y, Zhang L, Zhang Z, Gao F, Ji X, et al. A pH-responsive mesoporous silica nanoparticles-based multi-drug delivery system for overcoming multi-drug resistance. Biomaterials. 2011; 32: 7711-20.
3. Wu JL, Wang CQ, Zhuo RX, Cheng SX. Multi-drug delivery system based on alginate/calcium carbonate hybrid nanoparticles for combination chemotherapy. Colloids Surf., B. 2014; 123: 498-505.
4. Ahmed F, Pakunlu RI, Brannan A, Bates F, Minko T, Discher DE. Biodegradable polymersomes loaded with both paclitaxel and doxorubicin permeate and shrink tumors, inducing apoptosis in proportion to accumulated drug. J Controlled Release. 2006; 116: 150-8.
5. Miao J, Du YZ, Yuan H, Zhang XG, Hu FQ. Drug resistance reversal activity of anticancer drug loaded solid lipid nanoparticles in multi-drug resistant cancer cells. Colloids Surf., B. 2013; 110: 74-80.
6. Zhang L, Radovic-Moreno AF, Alexis F, Gu FX, Basto PA, Bagalkot V, et al. Co-delivery of hydrophobic and hydrophilic drugs from nanoparticle-aptamer bioconjugates. Chem Med Chem. 2007; 2: 1268-71.
7. Elumalai R, Patil S, Maliyakkal N, Rangarajan A, Kondaiah P, Raichur AM. Protamine-carboxymethyl cellulose magnetic nanocapsules for enhanced delivery of anticancer drugs against drug resistant cancers. Nanomed Nanotechnol Biol Med. 2015; 11: 969-81.
8. Chen Y, Jiang L, Wang R, Lu M, Zhang Q, Zhou Y, et al. Injectable smart phase-transformation implants for highly efficient *in vivo* magnetic-hyperthermia regression of tumors. Adv Mater. 2014; 26: 7468-73.
9. Kheirolomoom A, Lai CY, Tam SM, Mahakian LM, Ingham ES, Watson KD, et al. Complete regression of local cancer using temperature-sensitive liposomes combined with ultrasound-mediated hyperthermia. J Controlled Release. 2013; 172: 266-73.
10. Di Corato R, Bealle G, Kolosnjaj-Tabi J, Espinosa A, Clement O, Silva AK, et al. Combining magnetic hyperthermia and photodynamic therapy for tumor ablation with photoresponsive magnetic liposomes. ACS Nano. 2015; 9: 2904-16.
11. Ren Y, Zhang H, Chen B, Cheng J, Cai X, Liu R, et al. Multifunctional magnetic Fe_3O_4 nanoparticles combined with chemotherapy and hyperthermia to overcome multidrug resistance. Int J Nanomed. 2012; 7: 2261-9.
12. W-CH CCH, Lin YW, Yu TW, Chen HH, Lin SC, Chiang WH, Chiu HC. Active Tumor permeation and uptake of surface charge-switchable theranostic nanoparticles for imaging-guided photothermal/chemo combinatorial therapy. Theranostics. 2016; 6: 302-17.
13. Ryu JS, Raucher D. Elastin-like polypeptides: the influence of its molecular weight on local hyperthermia-induced tumor accumulation. Eur J Pharm Biopharm. 2014; 88: 382-9.
14. Al-Ahmady ZS, Chaloin O, Kostarelos K. Monoclonal antibody-targeted, temperature-sensitive liposomes: *in vivo* tumor chemotherapeutics in combination with mild hyperthermia. J Controlled Release. 2014; 196: 332-43.
15. Jayson GC, Kohn EC, Kitchener HC, Ledermann JA. Ovarian cancer. Lancet. 2014; 384: 1376–88.
16. Nossov V, Amneus M, Su F, Lang J, Janco JMT, RT Srinivasa, et al. The early detection of ovarian cancer: from traditional methods to proteomics. Can we really do better than serum CA-125?. Am J Obstet Gynecol. 2008; 199: 215-23.
17. Baumann KH, Wagner U, du Bois A. The changing landscape of therapeutic strategies for reccurrent ovarian cancer. Future Oncol. 2012; 8: 1135-47.
18. Pradhan L, Srivastava R, Bahadur D. pH- and thermosensitive thin lipid layer coated mesoporous magnetic nanoassemblies as a dual drug delivery system towards thermochemotherapy of cancer. Acta biomater. 2014; 10: 2976-87.
19. Gaikwad SM, Thakur B, Sakpal A, Singh RK, Ray P. Differential activation of NF-kappaB signaling is associated with platinum and taxane resistance in

MyD88 deficient epithelial ovarian cancer cells. Int J Biochem Cell Biol. 2015; 61: 90-102.
20. Swain AK, Pradhan L, Bahadur D. Polymer stabilized Fe_3O_4-graphene as an amphiphilic drug carrier for thermo-chemotherapy of cancer. ACS Appl Mater Interfaces. 2015; 7: 8013-22.
21. Chytil P, Hoffmann S, Schindler L, Kostka L, Ulbrich K, Caysa H, et al. Dual fluorescent HPMA copolymers for passive tumor targeting with pH-sensitive drug release II: impact of release rate on biodistribution. J Controlled Release. 2013; 172: 504-12.
22. Rengan AK, Bukhari AB, Pradhan A, Malhotra R, Banerjee R, Srivastava R, et al. *In vivo* analysis of biodegradable liposome gold nanoparticles as efficient agents for photothermal therapy of cancer. Nano Lett. 2015; 15: 842-8.
23. Jaiswal MK, Gogoi M, Sarma HD, Banerjee R, Bahadur D. Biocompatibility, biodistribution and efficacy of magnetic nanohydrogels in inhibiting growth of tumors in experimental mice models. Biomater Sci-Uk. 2014; 2: 370-80.
24. Jose S, Anju SS, Cinu TA, Aleykutty NA, Thomas S, Souto EB. *In vivo* pharmacokinetics and biodistribution of resveratrol-loaded solid lipid nanoparticles for brain delivery. Int J Pharm. 2014; 474: 6-13.
25. Jensen MM, Jorgensen JT, Binderup T, Kjaer A. Tumor volume in subcutaneous mouse xenografts measured by microCT is more accurate and reproducible than determined by 18F-FDG-microPET or external caliper. BMC Med Imaging. 2008; 8: 16.
26. Kruse AM, Meenach SA, Anderson KW, Hilt JZ. Synthesis and characterization of CREKA-conjugated iron oxide nanoparticles for hyperthermia applications. Acta biomater. 2014; 10: 2622-9.
27. Rao W, Zhang W, Poventud-Fuentes I, Wang Y, Lei Y, Agarwal P, et al. Thermally responsive nanoparticle-encapsulated curcumin and its combination with mild hyperthermia for enhanced cancer cell destruction. Acta biomater. 2014; 10: 831–842.
28. Ding H, Wu F. Image guided biodistribution and pharmacokinetic studies of theranostics. Theranostics. 2012; 2: 1040-53.
29. Nazir S, Hussain T, Ayub A, Rashid U, MacRobert AJ. Nanomaterials in combating cancer: therapeutic applications and developments. Nanomed Nanotechnol Biol Med. 2014; 10: 19-34.
30. LW QZ, Cheng R, Mao L, Arnold RD, Howerth EW, ZG C, Platt S. Magnetic nanoparticle-based hyperthermia for head & neck cancer in mouse models. Theranostics. 2012; 2: 113-21.
31. Mani J, Vallo S, Rakel S, Antonietti P, Gessler F, Blaheta R, et al. Chemoresistance is associated with increased cytoprotective autophagy and diminished apoptosis in bladder cancer cells treated with the BH3 mimetic (−)-Gossypol (AT-101). BMC Cancer. 2015; 15: 224.
32. Gong Y, Duvvuri M, Krise JP. Separate roles for the golgi apparatus and lysosomes in the sequestration of drugs in the multidrug-resistant human leukemic cell line HL-60. J Biol Chem. 2003; 278: 50234-39.
33. Larsen AK, Escargueil AE, Skladanowski A. Resistance mechanisms associated with altered intracellular distribution of anticancer agents. Pharmacol Ther. 2000; 85: 217–229.
34. Nicoletti MI, Lucchini V, Massazza G, Abbott BJ, D'Incalci M, Giavazzi R. Antitumor activity of taxol (NSC-125973) in human ovarian carcinomas growing in the peritoneal cavity of nude mice. Ann Oncol. 1993; 4: 151-5.
35. Nicoletti MI, Lucchini V, D'Incalci M, Giavazzi R. Comparison of Paclitaxel and Docetaxel Activity on Human Ovarian Carcinoma Xenografts. Euro J Cancer. 1994; 30: 691-96.
36. Iliopoulos D, Hirsch HA, Struhl K. Metformin decreases the dose of chemotherapy for prolonging tumor remission in mouse xenografts involving multiple cancer cell types. Cancer Res. 2011; 71: 3196-201.
37. Jin C, Li H, He Y, He M, Bai L, Cao Y, et al. Combination chemotherapy of doxorubicin and paclitaxel for hepatocellular carcinoma in vitro and in vivo. J Cancer Res Clin Oncol. 2010; 136: 267–274.